



Nonlinear Analyses in Rotordynamic Engineering

Joachim Schmied^(✉) and Andreas Fuchs^(✉)

DELTA JS AG Technoparkstrasse 1, 8005 Zurich, Switzerland
{jschmied, afuchs}@delta-js.ch

Abstract. Linear rotor-dynamic analyses such as Campbell diagrams of damped eigenvalues and unbalance response analyses are well established for the practical design layout of rotors. They are also required according to many standards such as API. Nonlinear analyses are widely avoided because of their complexity, even if they would be necessary for relevant practical answers. Sometimes questionable substitute linear analyses are carried out in such cases. In this paper four cases requiring nonlinear analyses are described: A vertical pump with water lubricated bearings, a turbocharger with semi-floating oil lubricated bearings, an electric motor with rolling element bearings running through a resonance and a Pelton turbine on tilting pad bearings losing two buckets. The vertical pump is linearly unstable, because of the unloaded bearings. The nonlinear analyses are necessary to receive the limit cycles of the unstable system. In case of the turbocharger the outer oil film of the semi-floating ring bearing is highly nonlinear and cannot be correctly described linearly. In case of the motor running through a resonance the dynamic bearing loads are very high, because the rolling element bearings are not able to provide much damping. The behavior then becomes nonlinear. Moreover, the bearing clearance can lead to nonlinear behavior, if the bearings are not preloaded. The blade loss for the Pelton turbine leads to nonlinear behavior due to the high dynamic bearing load.

Keywords: Non-linear phenomena in rotordynamics
Dynamic analysis and stability · Fluid film bearings · Rolling element bearings

1 Introduction

Nonlinear analyses are rarely carried out in practical engineering. There are good reasons for that: In many cases linear analyses are sufficient to get correct answers for the design of a machine although real machines are always nonlinear to some extent. Nonlinear analyses take considerable more effort than well-established linear analyses such as undamped critical speed maps, damped Campbell diagrams and damped unbalance response analyses. Most of these linear analyses are required by standards such as API standards [1], whereas so far, no standard asks for nonlinear analyses. Nonlinear analyses normally take a much bigger effort for the following reasons: The nonlinear effects must be modelled, analysis times are much longer (usually the nonlinear equations are integrated in the time domain by solvers such as Runge Kutta), the

solver may be numerical unstable, and the resulting behavior can be complex requiring some effort for the interpretation of the result.

In some cases, however, nonlinear analyses cannot be avoided for correct answers. Four such cases are described in this paper:

1. A vertical pump with water lubricated bearings: Fluid film bearings are normally linearized around their static load, which yield the linear stiffness and damping coefficients. The linearized behavior can give good results in a wide range of dynamic loads, not exceeding the static load. If the static load is zero or small, then strictly speaking the behavior is always nonlinear. Moreover, in the present example the rotor is unstable, because it has unloaded cylindrical bearings. A linear analysis does not tell at which level the unstable system (limit cycle) stabilizes. To get this result, which is essential for an assessment of the rotor behavior, a nonlinear analysis is necessary.
2. A turbocharger with semi-floating ring bearings: The outer oil film of bearings functions as a squeeze film damper without centering device (e.g. a squirrel cage) for the ring. The behavior of such a damper is essentially nonlinear, because a centering force for the ring only arises by a vibration of the ring. Therefore, only a nonlinear analysis can correctly simulate such a rotor. For the investigated turbocharger, which is also described in [2], extensive measurements were made by the vendor ABB. The analyses are compared to these measurements.
3. An electric motor with rolling element bearings running through a resonance: In contrast to fluid film bearings rolling element bearings do not provide notable damping. Without additional damping device such as a squeeze film damper, rotors supported on rolling element bearings are therefore not suited to run in resonance or even above a critical, which requires crossing it. The latter may be acceptable in case of sufficient acceleration. Practically such applications exist. The example here is derived from a real motor not running above a critical. Nevertheless, we will demonstrate the effects arising when crossing the critical with this example. Since the damping is low, high vibrations and high dynamic bearing forces arise, which require a nonlinear analysis. Linearized bearing characteristics around a static equilibrium are no longer applicable.
4. A vertical Pelton turbine on tilting pad oil bearings losing three buckets: The loss of two buckets causes large dynamic forces requiring a nonlinear analysis. The results of the nonlinear simulation are compared to linear results.

All examples are practically relevant. The investigated turbocharger corresponds to a built machine, which has been measured. The other examples are derived from real applications. Crossing of resonances on ball bearings without damping device is practically done, although not for the type of motor investigated here. The speed range of the electric motor has been extended to show the corresponding effects.

All analyses were carried out with the comprehensive rotordynamic program MADYN 2000 [3].

2 Nonlinearities and Solving the Nonlinear Equations

2.1 Nonlinear Fluid Film Bearings

The nonlinear fluid film forces on the rotor are described in a 2, 3-coordinate system according to Eqs. (1) and (2) as a function of the rotor position (see Fig. 1).

$$-\begin{bmatrix} F_3 \\ F_2 \end{bmatrix} = SoFactor \left(\begin{bmatrix} So(\varepsilon, \gamma) \sin \alpha \\ So(\varepsilon, \gamma) \cos \alpha \end{bmatrix} + \begin{bmatrix} \beta_{33}(\varepsilon, \gamma) & \beta_{32}(\varepsilon, \gamma) \\ \beta_{32}(\varepsilon, \gamma) & \beta_{22}(\varepsilon, \gamma) \end{bmatrix} \frac{1}{\Delta R \Omega} \begin{bmatrix} \dot{x}_3 \\ \dot{x}_2 \end{bmatrix} \right) \quad (1)$$

$$SoFactor = \frac{F}{So} = \frac{BD\eta\Omega}{\Psi^2} \quad (2)$$

with So as the Sommerfeld number, β as dimensionless damping coefficients, ΔR as the radial minimum clearance, ε as the dimensionless eccentricity with reference ΔR , γ as the position angle, Ω as the rotor speed \dot{x} as the rotor velocities, B as the bearing width, D as the bearing diameter, η as the fluid viscosity, and Ψ as the dimensionless bearing clearance $2\Delta R/D$.

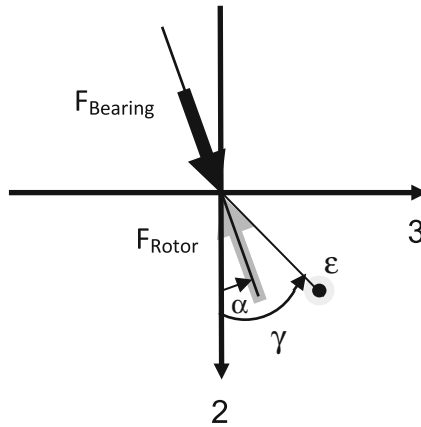


Fig. 1. Coordinate system to describe the bearing force and its direction as a function of the rotor position described by the eccentricity ε and position angle γ .

As can be seen the force is split into two parts: one part is caused by rotation of the journal (the part described by the So-number) and the other by lateral movements (the part described by the damping coefficients). Both parts are calculated by solving the Reynolds equation. The energy equation is solved simultaneously for the temperature distribution unless an analysis with constant temperature is carried out. Various effects such as turbulence and 2-phase flow in cavitation zones can be considered (see [4]). A simplified analysis neglecting turbulence and assuming iso-viscous fluid according to a mean temperature as it is described in the DIN standard [5] is also possible. The solution is done for a grid of journal positions ε, γ within the possible clearance range. Both parts of the force are highly dependent on ε, γ and thus nonlinear.

For the calculation of run-ups, the bearing analysis according to DIN is especially suited, since the Sommerfeld similarity applies for this analysis type. The speed dependence of the bearing characteristic then can be fully considered by the dimensionless damping coefficients and the Sommerfeld number, which varies with the speed. There is no additional dependency such as the Reynolds number for turbulence, which cannot be considered for this analysis type. In many applications turbulences plays a minor role.

2.2 Nonlinear Rolling Element Bearings

The rolling element bearing forces are calculated with the help of the Hertzian theory as described in ISO/TS 16281 and DIN 26281, respectively (see [6]). The forces due to Hertzian pressure can be linearized for small dynamic forces near large static forces. However, they are basically nonlinear. Moreover, dynamic loads for many bearing types such as deep groove or angular contact ball bearings can change the contact angles between the balls and the inner and outer race, which contributes to a nonlinear behavior. The bearing clearance can also cause nonlinear behavior. Additionally, a coupling between the axial and radial direction occurs for many bearing types as the above-mentioned ball bearings. The bearing forces the two radial directions 2 and 3 and moments about these axes as well as the axial force as a function of the radial and axial displacements and tilting angles about the radial axes are calculated in a routine according to the above-mentioned theory, which is provided by MESYS (see [7]).

Rolling element bearings provide almost no damping force. Nevertheless, a damping force can be considered in MADYN 2000 for harmonic response analyses by a damping matrix, which is proportional to the stiffness matrix of the statically loaded bearing. The stiffness matrix describes the linearized forces. The factor is calculated according to Eq. (3). It yields a damping according to a defined damping ratio at the exciting frequency.

$$\mathbf{D} = \frac{2D}{\omega} \mathbf{K} \quad (3)$$

with the \mathbf{D} as the damping matrix, \mathbf{K} as the stiffness matrix of the rolling element bearing, D as a damping ratio to be defined and ω as the exciting frequency. The matrices are 5×5 matrices for the two radial displacements, the two tilting angles about the radial axes and the axial displacement.

A similar damping force can be used in non-linear transient analyses. The damping matrix then is calculated with a reference frequency, which can be the speed or a specifically defined frequency.

2.3 Solving the Nonlinear Equation

For solving the system of nonlinear equations, the nonlinear bearing forces are put on the right-hand side as shown in Eq. (4).

$$\begin{bmatrix} \ddot{\mathbf{x}} \\ \dot{\mathbf{x}} \\ \dot{\mathbf{q}} \end{bmatrix} = \begin{bmatrix} -\mathbf{M}^{-1}(\mathbf{D} + \mathbf{G}) & -\mathbf{M}^{-1}\mathbf{K} & \mathbf{A}_{xq} \\ \mathbf{E} & \mathbf{0} & \mathbf{0} \\ \mathbf{A}_{qx} & \mathbf{A}_{qx} & \mathbf{A}_{qq} \end{bmatrix} \begin{bmatrix} \dot{\mathbf{x}} \\ \mathbf{x} \\ \mathbf{q} \end{bmatrix} + \begin{bmatrix} \mathbf{M}^{-1}\mathbf{F}(t) \\ \mathbf{0} \\ \mathbf{0} \end{bmatrix} + \begin{bmatrix} \mathbf{F}_{NL}(\mathbf{x}, \dot{\mathbf{x}}) \\ \mathbf{0} \\ \mathbf{B}_q \end{bmatrix} \quad (4)$$

In Eq. (4) \mathbf{M} is the mass matrix, \mathbf{D} the damping matrix, \mathbf{G} the gyroscopic matrix, \mathbf{K} the stiffness matrix and \mathbf{E} the unit matrix. The vector \mathbf{x} contains structural coordinates of the rotor and support system modelled in MADYN 2000. Supports can also be imported in the form of state space systems, which have the additional coordinates \mathbf{q} (see for example [8, 9]). The sub-matrices \mathbf{A}_{ij} describe the coupling of MADYN 2000 coordinates to the imported state space supports. These matrices are created with the help of the support system matrix, observer and control matrix. Certain bearing types such as magnetic bearings or full models of tilting pad bearings may also have additional coordinates (see for example [10]). The examples of the present paper do not have such bearings and the additional coordinates are not included in Eq. (4). \mathbf{F} is the vector of external exciting forces, which can only be applied to structural MADYN 2000 coordinates and \mathbf{F}_{NL} the vector of nonlinear forces. The stiffness matrix \mathbf{K} and damping matrix \mathbf{D} as well as the sub-matrices \mathbf{A}_{ij} may contain linear bearing coefficients, if some bearings are treated as linear. The vector \mathbf{B}_q describes the forces on the state space stator system. It is created with the help of the state space observer and control matrix.

Equation (4) can also be written in the following form:

$$\dot{\mathbf{z}} = \mathbf{A}\mathbf{z} + \mathbf{B}(t) + \mathbf{B}_{NL}(\mathbf{x}, \dot{\mathbf{x}}, \mathbf{q}) \quad (5)$$

Before solving the equation by integration with a Runge Kutta solver, it is bi-modally reduced with the help of the complex left and right eigenvectors of the system $\Phi_L \Phi_R$ as shown in Eq. (6).

$$\Phi_L' \dot{\mathbf{z}} \Phi_R = \Phi_L' \mathbf{A} \Phi_R + \Phi_L' \{ \mathbf{B}(t) + \mathbf{B}_{NL}(\mathbf{x}, \dot{\mathbf{x}}, \mathbf{q}) \} \quad (6)$$

The linear part thus is decoupled. The method is described in detail in [11] and summarized in [12]. The resulting system to solve is as follows:

$$\dot{\mathbf{w}} = \mathbf{A}\mathbf{w} + \Phi_L' \{ \mathbf{B}(t) + \mathbf{B}_{NL}(\mathbf{x}, \dot{\mathbf{x}}, \mathbf{q}) \} \quad (7)$$

with

$$\mathbf{z} = \Phi_R \mathbf{w} \quad (8)$$

The matrix \mathbf{A} hereby is the diagonal matrix of the considered eigenvalues of the linear system.

The linear system is speed dependent; hence the eigenvalues and matrices of the eigenvectors are also speed dependent. For the analyses of a run up or down, the matrices are created for a suitable number of speed steps and then interpolated during the solution of the equation for each time step.

3 Vertical Pump with Cylindrical Water Lubricated Bearings

3.1 Description of the Model

The model of the vertical pump is shown in Fig. 2. The complete length of the assembly is about 12 m. The upper part with a motor is on the left side. The pump has only one impeller at the bottom shown on the right side. The pump rotor is shaded in blue. The casing of the pump, which is a pipe, is modelled as a shaft with zero speed. It is shaded in grey (partly visible as a black line). The pipe is fixed to a foundation, which is denoted as customer support in the model. It consists of a flange of the pipe. The flange is fixed with general springs to the ground. The general springs represent the stiffness of the foundation and introduce anisotropy to the system. The motor rotor is not modelled as part of the shaft, since it is coupled to the pump shaft with a flexible coupling. The whole motor including its housing is modelled as a rigid mass fixed to the flange at the customer support stiffness (the sphere in Fig. 2). The distance of the center of gravity to the support is bridged with a rigid element.

The pump shaft is supported in the pipe with an angular contact rolling element bearing, which also carries the axial load. The upper bush and casing bearing are closed cylindrical bearings. The other bush bearings are cylindrical bearings with 3 equal pads and a deep groove between the pads. The ambient pressure of the upper bush bearing corresponds to the pump discharge pressure of 10 bar. For the other bush bearings and the casing bearing the Archimedes hydrostatic pressure adds to the discharge pressure, which is about 1 bar for the lowest bearing. The elevated ambient pressure influences the cavitation, which is considered in the bearing model with a 2-phase model (see [2, 4]). A contact stiffness to account for a surface roughness of 10 μm has been considered for all bearings according to the model in [13].

An added mass for the pipe is considered. The mass of the enclosed water is added. For the rotor an added mass according to the formula (9) published in [14] has been used to estimate the effect. It yields a mass of about 3% of the rotor mass and therefore is neglected.

$$\mu = \pi\delta \frac{OD^3}{8s} \tag{9}$$

with μ as the added mass per length, δ as the density, OD as the rotor outer diameter and s as the radial clearance, which is very large for our case (≈2 OD).

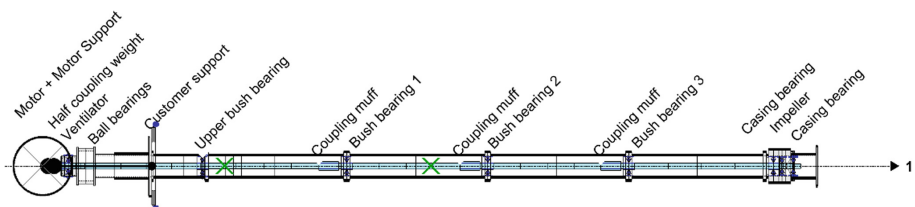


Fig. 2. Model of the vertical pump

3.2 Linear Behavior, Campbell Diagram

The Campbell diagram for a speed range up to 150% speed and a frequency range to 50 Hz, which corresponds to two times nominal speed can be seen in Fig. 3. The corresponding mode shapes can be seen in Fig. 4. Note, that the colors for corresponding modes are the same in both figures. The dashed line in the shape plot represents the pipe deformation and the solid line to the rotor deformation. The shapes are shown in two projections at the instant when the maximum deflection occurs. The two planes for the projections are indicated in the plot next to the shape plot. The first projection with the fat line is into the plane defined by the maximum deflection and the rotor axis, the second projection with the thin line into the perpendicular plane. The whirling direction and mean global orbit shape (also see [3]) are indicated as well.

Parameter Variation Analysis

Type: Campbell Diagram
 Analysis: 11-Jul-2017 14:42 - 18 rel.speeds (0.15...1.5), bearing loads from SAN

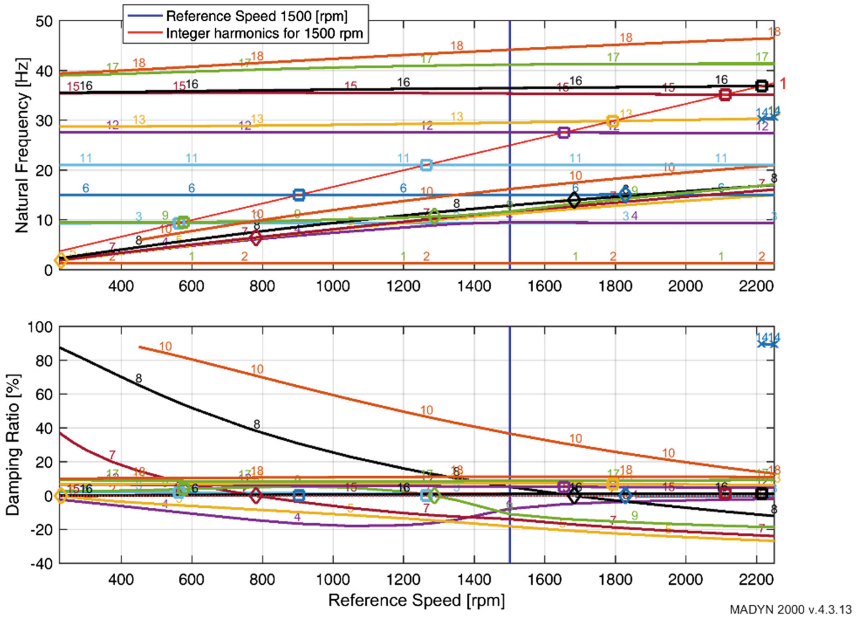


Fig. 3. Campbell diagram with eigenvalues

The first two modes are a cantilever like bending of the pipe and the rotor in two perpendicular directions. There is almost no relative displacement between rotor and pipe. The next modes are bending modes of the rotor with increasing order and increasing relative displacement. The modes appear as elliptically forward and backward whirling modes. They are elliptic due to the anisotropy of the support stiffness. The forward modes with relative displacement become unstable (mode 4, 5, 7, 9) if their frequency is below 50% speed, which is the whirling speed of the fluid in the cylindrical bearings.

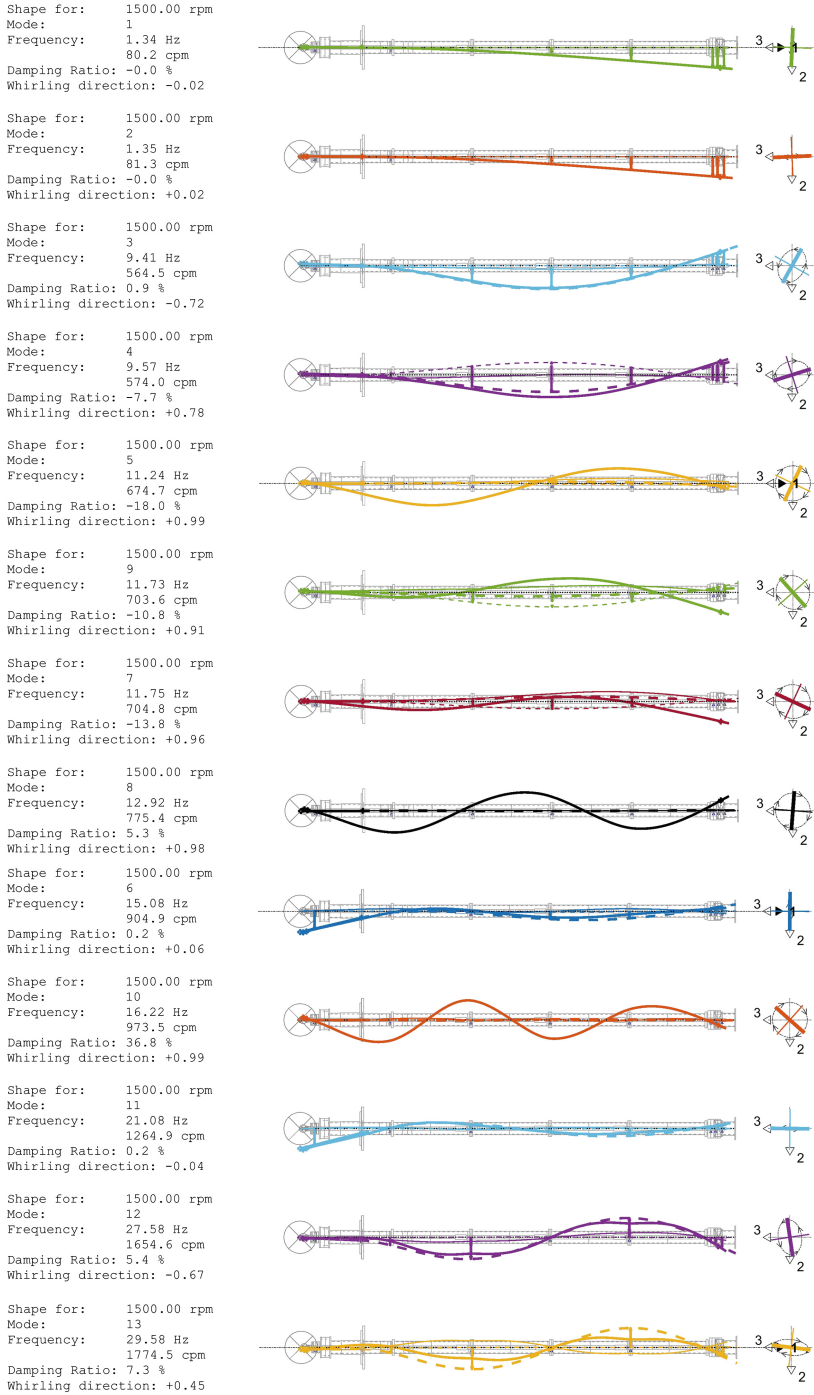


Fig. 4. Natural modes at nominal speed 1500 rpm

3.3 Results of a Nonlinear Run Up Analysis

Since the linear system is unstable, a nonlinear analysis must be carried out to determine limit cycles revealing a realistic vibration level of the rotor. A nonlinear run up analysis with an unbalance of G10 at the impeller has been carried out. The reference mass for the G value is the rotor section at the impeller. The run up has been carried out from 10% to 110% speed in 60 s, which is almost stationary for this system.

Results of this analysis can be seen in the following figures: The absolute displacements of the pipe at the bearing locations in Fig. 5, the orbits of the relative displacements in the fluid bearings in Fig. 6 and the 3D shape at 1500 rpm in Fig. 7.

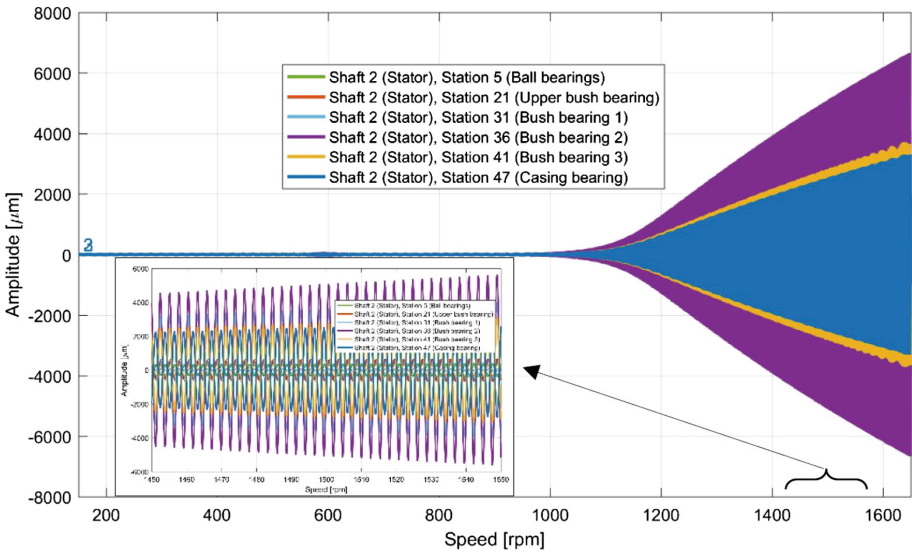


Fig. 5. Absolute vibrations of the pipe at bearing locations

The vibrations of the pipe indeed are huge. At 1500 rpm, 100% speed the level at bush bearing 2 is several mm. The shape at about 1500 rpm in Fig. 7 corresponds to the 2nd bending, mode 4 in Fig. 4. The by far dominating frequency is about 10 Hz, which approximately corresponds to the frequency of this mode. The vibration level at the ball bearing in the top is much lower. At 1500 rpm it is about 300 µm, which corresponds to a still high rms value of 33 mm/s. This is the location where vibrations of such machines are typically measured. Other locations with bearings are difficult to access.

The relative vibration level in the fluid bearings at nominal speed in Fig. 6 is about 90% of the bearing clearance for all bearings without considering the surface roughness, which means, that the contact stiffness just begins to become effective.

The force at nominal speed in bush bearing 2 is about 2400 N corresponding to a specific dynamic load of 3 bar.

The vibration behavior of the pump as presented here is not acceptable or at least at the limit. The surrounding water, which is not considered in the analysis, probably helps attenuating the vibration, especially at such levels as calculated here.

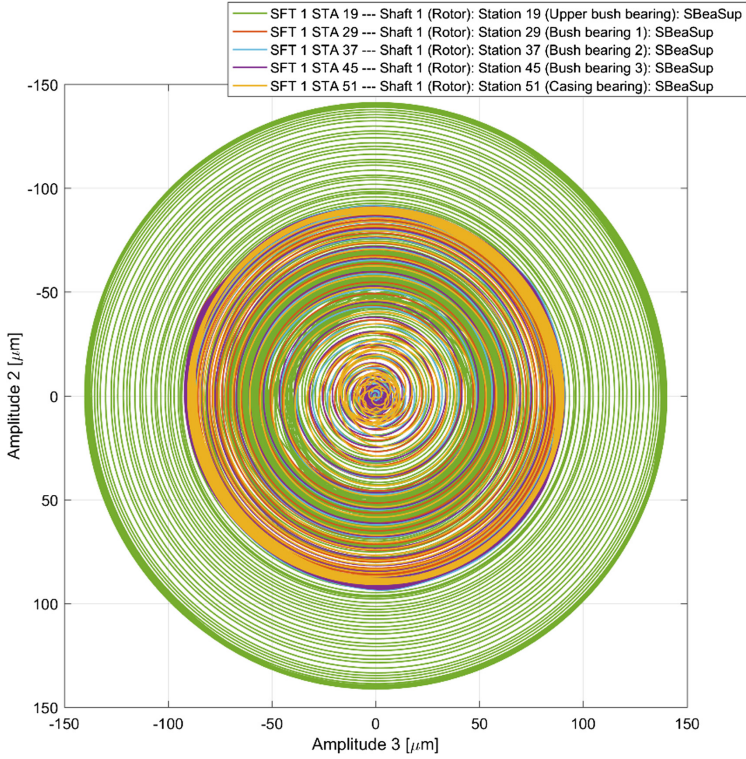


Fig. 6. Orbits of relative vibrations in the fluid bearings

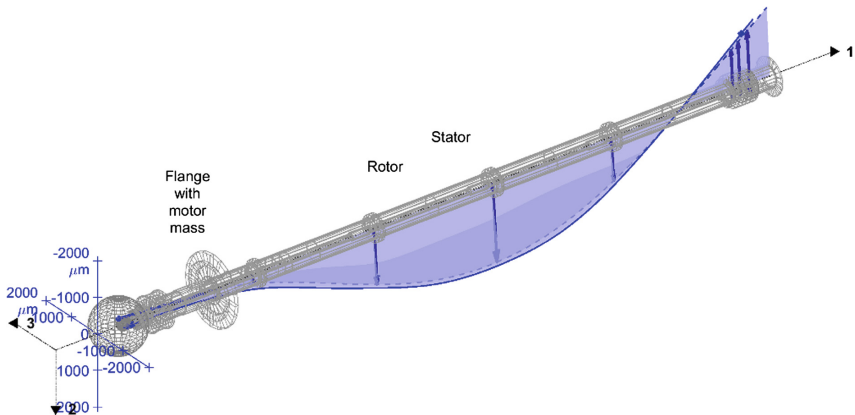


Fig. 7. Shape at nominal speed of 1500 rpm

4 Turbocharger with Semi-floating Ring Bearings

4.1 Description of the Model

The structure of the rotor model is shown in Fig. 8. The rotor is supported in two semi-floating ring bearings, which are shown in Fig. 9. The casing is considered as rigid, since it is very stiff compared to the rather soft support.

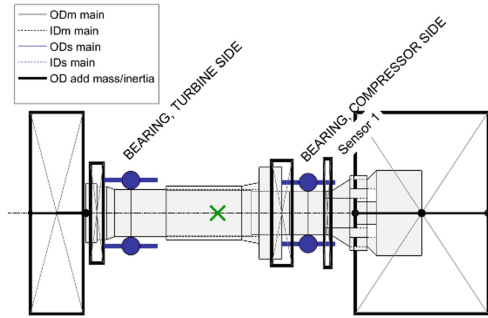


Fig. 8. Model of the turbocharger

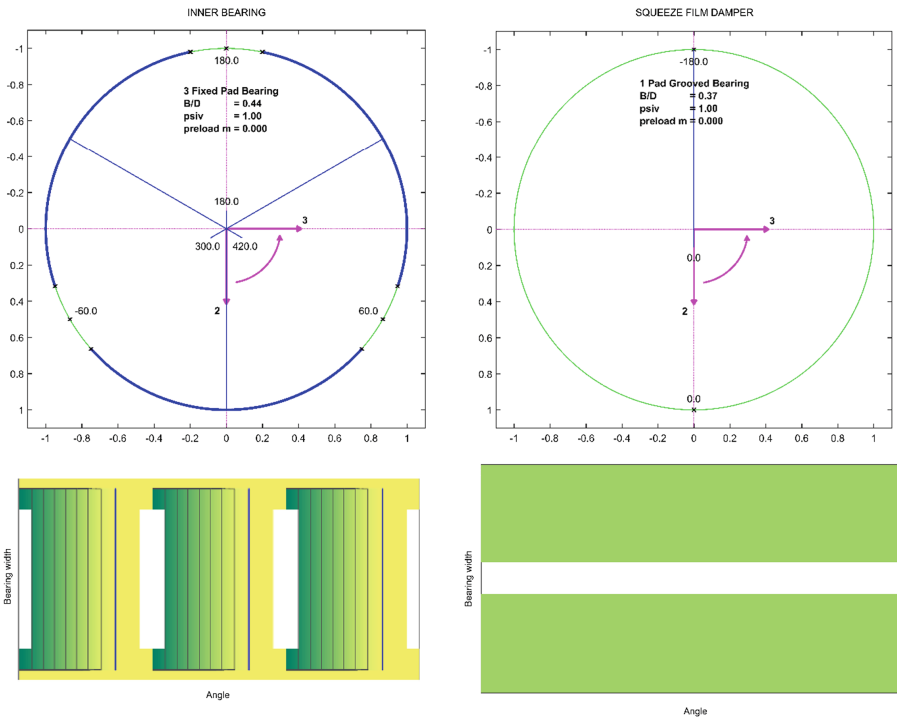


Fig. 9. Geometry and clearance of the semi-floating ring bearings, left inner film, right outer squeeze film

The inner film of the floating ring bearing has three hydrodynamic pockets, which are machined in the non-rotation ring. The outer film is plain cylindrical with a central groove distributing the oil. The outer film functions as a squeeze film.

The non-linear bearing characteristics were calculated according to DIN. Speed dependent oil temperature and thermal expansion of the ring and casing are considered. The speed dependence of the temperature and thus the viscosity as well as the clearance change influence the bearing characteristics through the Sommerfeld number.

4.2 Results of a Nonlinear Run Up Analysis with a Comparison to Measurements

The run up is calculated from 10% to 120% speed. The run up time is 10 s. The orbits of the rotor journal relative to the ring as well as the ring orbits are shown in Fig. 10. Measured and calculated vibration spectra are shown in Fig. 11.

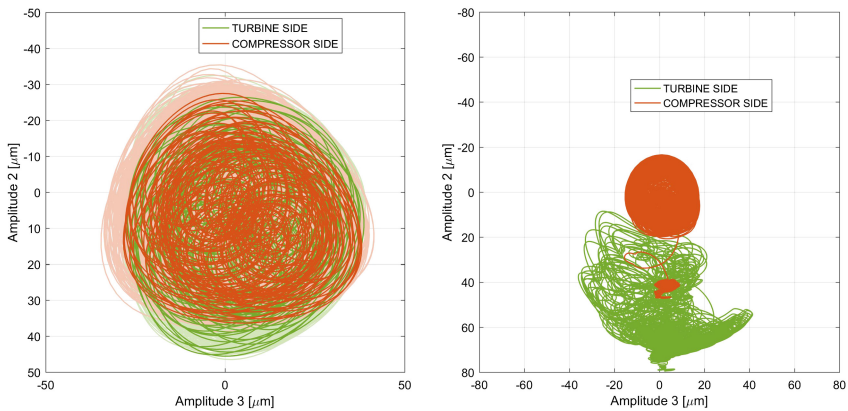


Fig. 10. Orbits of the rotor relative to the ring (left) and the ring (right)

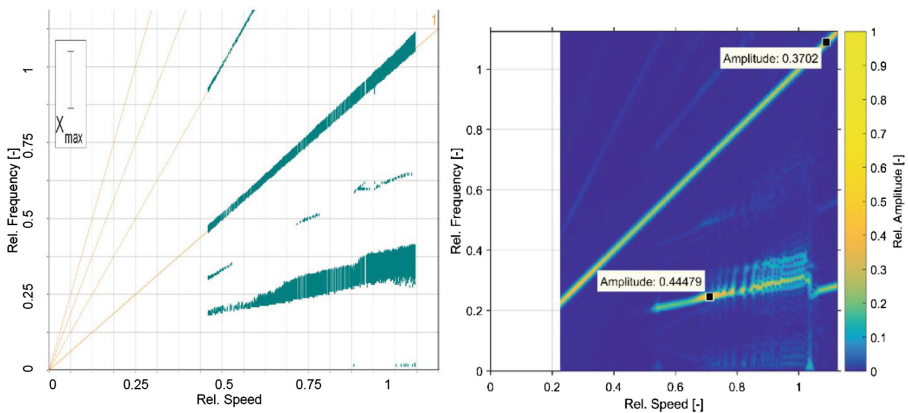


Fig. 11. Spectrogram of the run up at sensor 1 (left measurement, right simulation)

The squeeze film of the outer ring is completely free. It has no centering device such as a squirrel cage. A centering force is only created by vibrations of the ring. In the right plot of Fig. 10 the centering effect can be clearly seen. At low speed the two rings have a large eccentricity corresponding to the outer film clearances, which are different for the two bearings. With increasing speed and increasing vibration they are centered. On the compressor side the centering occurs in two stages. The 2nd stage is caused by a sudden change of pattern of the sub-synchronous vibration at about 100% speed, which can be seen in the calculated spectrum in Fig. 11.

The measured and calculated spectrograms clearly show the synchronous and sub-synchronous vibration amplitudes. A component with twice the frequency of each of the dominating frequency can also be seen. The agreement regarding frequency and amplitude between measurement and calculation is very good.

5 Motor with Deep Groove Contact Rolling Element Bearings

5.1 Description of the Model

The rotor with deep groove rolling element bearings can be seen in Fig. 12. The outer races of the deep groove ball bearings are modelled as shafts. The rolling element bearings connect the shaft and the outer races. Since for deep groove bearings the axial direction, radial direction as well as the rotation about the radial axes are coupled, all bending degrees of freedom as well as the axial degree of freedom are considered. The outer rings have only axial degrees of freedom, i.e. they are radially rigid. An axial preload is applied to the left bearing A. Bearing A is axially free, its outer ring is supported in axial direction by a weak axial spring. The outer ring of the right bearing B is rigidly supported in axial direction. It is an axially fixed bearing.

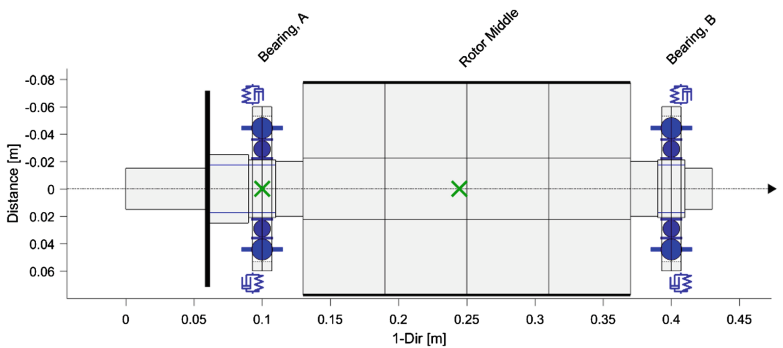


Fig. 12. Rotor with rolling element bearings

The speed dependence of the bearings due to centrifugal and gyroscopic forces of the rolling elements is considered.

5.2 Linear Behavior, Campbell Diagram

The Campbell diagram and mode shapes in the critical speeds for linearized bearing characteristics is shown in Fig. 13. The linearization is about the statically loaded bearings due to the weight and an axial preload of 700 N.

As can be seen the bending critical (mode 3 forward whirling) is above 100% speed, which is typical for rotors on rolling element bearings, since running through a critical is a problem with the poor damping, that this bearing type can provide. Beside the bending critical there is an axial mode, with a resonance close to nominal speed.

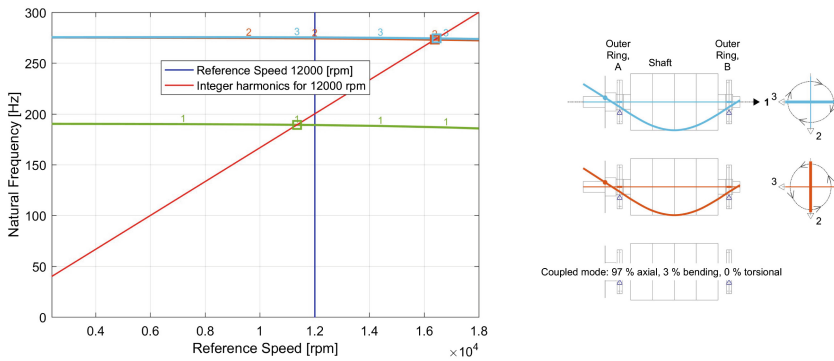


Fig. 13. Campbell diagram and shapes in the critical speeds

5.3 Results of a Nonlinear Run Up Analysis

A run up from 20% to 160% speed within 5 s for an unbalance in the middle of the rotor with a level of G2.5 has been calculated for this system with non-linear bearing properties. During the run up the critical speed is crossed, which is not foreseen for this machine, but envisaged in other cases.

The vibrations at the bearings in radial and axial direction are shown in Figs. 14 and 15. They reveal some remarkable behavior. The critical is lower than expected according to the Campbell diagram. The maximum vibration occurs at about 15500 rpm, whereas the critical in the Campbell diagram is at 16500 rpm. The axial resonance can be seen in the axial vibration at a speed where it can be expected according to the linear analysis. In the radial resonance large axial fluctuations occur combined with an axial shift, which can be explained as follows and which also explains the lower critical speed.

Due to the high radial loading of the bearing when approaching the resonance, the balls of the bearing seek a more centered position in the groove, which results in an axial shift of the shaft and a new contact angle. The new contact angle yields a lower stiffness despite the high radial load. In [15] this is explained more in detail including the change of stiffness due to the different contact angle.

Due to the axial preload the bearing does not have clearance in axial direction. In case of no preload further nonlinear effects can occur, which are described in [15].

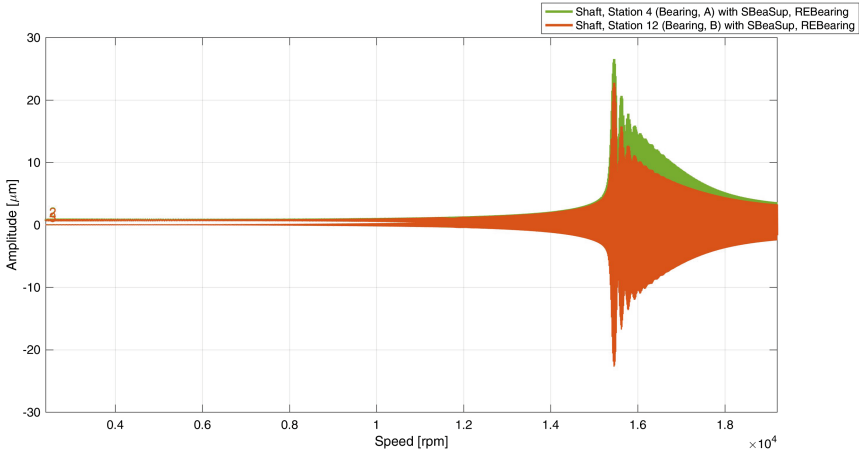


Fig. 14. Displacements in radial 2- and 3-direction at the bearings during run up

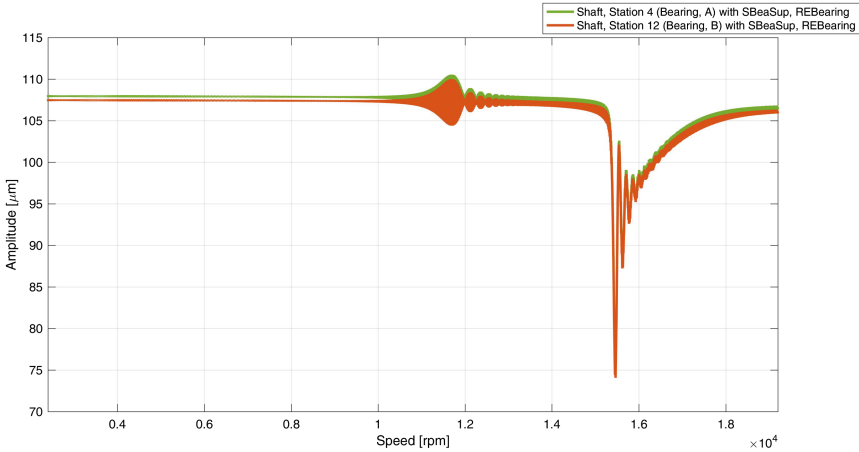


Fig. 15. Displacement in axial direction at the bearings during run up

6 Loss of Three Buckets of a Pelton Turbine

6.1 Description of the Model

The model for a vertical Pelton turbine is shown in Fig. 16. The Pelton runner is modelled as a rigid disk on the left side of the rotor. In the middle of the rotor is a generator. The rotor is supported on fluid film bearings. The bearing on the left turbine side is also shown in Fig. 16. It is a tilting pad bearing with 8 pads. In the model this bearing has a spring mass support representing the foundation. Its natural frequency is far above running speed and the rotor bending frequency. On the right side the bearing and support are modelled by a substitute spring. The turbine bearing is loaded with a static lateral force caused by the water jet.

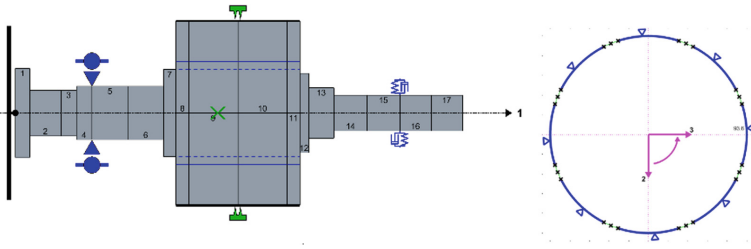


Fig. 16. Model of a vertical Pelton turbine with the geometry of the turbine bearing

6.2 Results of the Nonlinear Analysis of the Bucket Loss, Comparison to Linear Results

The bucket loss is calculated by suddenly applying a rotation force at nominal speed to the Pelton runner corresponding to the centrifugal force. In our case this force is 4.5 times the static jet force of 1000 kN. The initial condition for the analysis is the static equilibrium position due to the force from the water jet at the turbine. The turbine is running below its 1st bending mode. The separation margin is 45%.

The results of the analysis with a nonlinear turbine bearing can be seen in Fig. 17. For the orbit a comparison to a linear analysis is shown, with a linearization of the turbine bearing about its static equilibrium.

In case of the nonlinear analysis the orbit remains within the bearing clearance. It follows the bearing contour. At the pad pivot points the deflection is 85% of the minimum bearing clearance. Note, that 10 μm surface roughness is considered in the nonlinear analysis. For the linear analysis the deflections by far exceed the bearing clearance.

In the shape in Fig. 17 the arrow at the turbine bearing indicates the displacement of the support. It can be seen, that the relative displacement in the bearing is very small compared to the support displacement, which is almost 8 mm.

The maximum force on the turbine support is 13000 kN. The values are practically equal for the linear and nonlinear analysis. This applies for this model with a rather simple support structure and rather stiff rotor. It cannot be generalized.

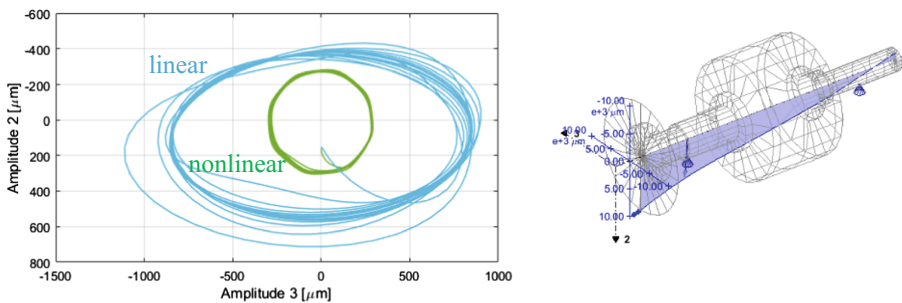


Fig. 17. Linearly and nonlinearly calculated orbit after a bucket loss, shape of nonlinear analysis at the instant of maximum deflection

7 Summary

Four examples are presented requiring unpopular nonlinear rotordynamic analyses for different reasons. In all examples the nonlinearity is in the bearings. For a vertical pump, which is linearly unstable, the nonlinear analysis is necessary for determining limit cycles. In case of a turbocharger with semi-floating ring bearings the reason for a nonlinear analysis is the essential nonlinear behavior of the outer oil film, which functions as a squeeze film damper without centering device. A motor rotor on rolling element bearings running through a resonance requires nonlinear analyses, because of the large forces, which change contact angles and do no longer allow linearizing the Hertzian pressure. For the simulation of a bucket loss of a Pelton turbine with an 8-tilting pad fluid film bearing on the turbine side, the necessity for a nonlinear analysis again arises due the large bearing forces, exceeding the static load by a factor of 4.5.

References

1. API Recommended Practice 684, 2nd edn (2005)
2. Fuchs, A., Klimpel, T., Schmied, J., Rohne, K.: Comparison of measured and calculated vibrations of a turbocharger. In: Proceedings of SIRM, 12th International Conference on Vibrations in Rotating Machines, Graz, Austria (2017)
3. MADYN 2000 program documentation (2017)
4. Fuchs, A.: Schnelllaufende Radialgleitlagerungen im instationären Betrieb. Dissertation TU Braunschweig (2002)
5. DIN 31 657. Hydrodynamische Radial-Gleitlager im stationären Betrieb. Berechnung von Mehrflächen und Kippsegmentlagern. Beuth Verlag, Berlin (1992)
6. ISO/TS 16281: Rolling bearings – Methods for calculating the modified reference rating life for universal loaded bearings (2008)
7. MESYS. http://www.mesys.ch/doc/MESYS_Rolling_Bearing_Calculation.pdf
8. Krüger, T., Liberatore, S., Knopf, E.: Complex substructures and their impact on rotordynamics. In: Proceedings of SIRM, 10th International Conference on Vibrations in Rotating Machines, Berlin, Germany (2013)
9. Schmied, J., Perucchi, M.: Coupled rotor-bearing-casing analysis. In: 22nd Swiss CADFEM ANSYS Simulation Conference (2017)
10. Schmied, J., Fedorov, A., Grigoriev, B.: Nonsynchronous tilting pad bearing characteristics. In: Proceedings of the 8th IFToMM International Conference on Rotordynamics, Seoul Korea (2010)
11. Nordmann, R.: Ein Näherungsverfahren zur Berechnung der Eigenwerte und Eigenformen von Turborotoren mit Gleitlagern, Spalterregung, äusserer und innerer Dämpfung. Dissertation TU Darmstadt (1974)
12. Krämer, E.: Dynamics of Rotors and Foundations. Springer, Heidelberg (1993)
13. Greenwood, J.A., Williamson, J.B.P.: Contact of normally flat surfaces. In: Proceedings of the Royal Society of London, Series A, Mathematical and Physical Sciences, vol. 295, no. 1442 pp. 300–319 (1966)
14. Amoser, M.: Strömungsfelder und Radialkräfte in Labyrinthdichtungen hydraulischer Strömungsmaschinen. Dissertation ETH Zurich Nr. 11150 (1995)
15. Delta JS. http://www.delta-js.ch/file/344/MADYN_2000_Release_43_Nonlinear_REB.pdf